Australian Meteorological and Oceanographic Journal 64 (2014) 27–35

Secondary circulations in rotating-flow boundary layers

Richard Rotunno
National Center for Atmospheric Research[1]
(Manuscript received July 2013; revised November 2013)

The *rotating-flow boundary layer* is a special case of the more general three-dimensional boundary layer in which the pressure gradient imposed by the outer flow (above the boundary layer) is not in the same direction as the outer flow. The rotating-flow boundary layer thus has motion that is transverse to the streamlines of the outer flow, that is, there is a *secondary circulation* to the primary circulation of the outer flow. That the secondary circulation can extend far above the boundary layer presents a set of perplexing conceptual problems unlike any encountered in a two-dimensional boundary layer. This paper reviews, critically discusses and presents numerical simulations attempting to supplement existing theory for several canonical problems concerning secondary circulations in rotating-flow boundary layers. Based on the present results, brief comments on atmospheric vortices are made.

Introduction

Atmospheric vortices such as tornadoes, waterspouts, dust devils, hurricanes and midlatitude cyclones are influenced by the impermeable frictional boundary that is the Earth's surface. In each case there is a rotating-flow boundary layer with secondary circulations having effects on the primary flow ranging from modest to significant. In the mid-latitude cyclone, the importance of the Ekman layer in transporting fluid in and out of the atmosphere above is relatively well understood (Pedlosky 1984, Chapter 4). At the other end of the size spectrum, the distinctive properties of tornado boundary layers in producing very intense swirling motions near the ground are also well recognized (Rotunno 2013). Studies of steady-state hurricane boundary layers indicate that they possess features of both: for example in the Emanuel (1986) theory, the hurricane's secondary flow is essential for bringing latent heat and angular momentum into the hurricane's interior, gradient-wind-balanced primary circulation; on the other hand, such boundary layers may have intense radial-wind accelerations and supergradient tangential winds (Smith and Montgomery 2008; Bryan and Rotunno 2009).

In terms of the basic fluid mechanics, secondary circulations not involving density gradients are the most well understood; and of these flows, the ones that are in near solid-body rotation are best understood (Duck and Foster 2001). The aim of the present work is to revisit a constant-density flow that is far from solid-body rotation (as in tornadoes) and to help complete its description for laboratory-relevant bounded domains. A firm understanding of the secondary circulations occurring in this flow may help in the development of improved theories for more complex geophysical vortices such as hurricanes.

[1] The National Center for Atmospheric Research is sponsored by the National Science Foundation.

Corresponding author address: Richard Rotunno, National Center for Atmospheric Research. Email: rotunno@ucar.edu.

History

Solid-body-rotation outer flow

The earliest and simplest canonical problem in this general category is the flow above an infinite rotating disk solved for by von Kármán in 1924 (see pp. 93–99 of Schlichting 1968). The no-slip condition at the disk requires the tangential flow be in solid-body rotation at the lower surface ($v=\omega r$), where ω is the disk rotation rate and r the radius); the similarity solutions developed by von Kármán,

$$u=\omega rF(\zeta) \quad , \quad v=\omega rG(\zeta) \quad , \quad w=\sqrt{\nu\omega}H(\zeta) \quad ...(1)$$

Figure 1a indicates that the tangential flow decays monotonically with distance $\zeta = z\sqrt{\omega/\nu}$ above the disk, where ν is the kinematic viscosity; the radial flow at $u \geq 0$ all levels with a maximum at $\zeta \approx 0.9$. As $\zeta \to \infty, (F,G) \to (0,0)$ but the axial velocity approaches a negative constant ($H \to -0.886$) indicating flow towards the disk at large distance from the disk.

Fig. 1. Depiction of similarity solutions for an unbounded (a) flow above a rotating disk (von Kármán), and (b) flow in solid-body rotation above a stationary disk (Bödewadt). (After Schlichting 1968.)

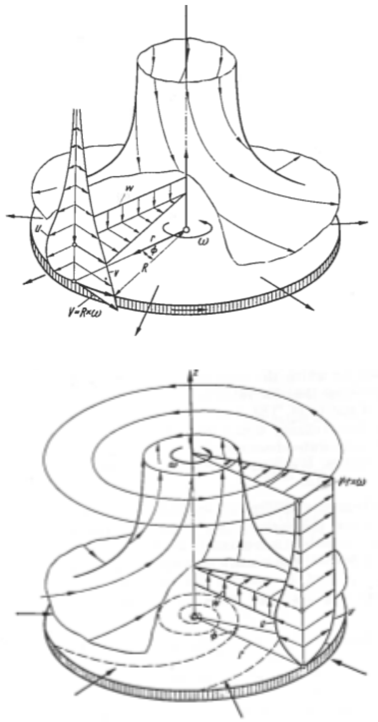

(a)

(b)

Although this secondary circulation in von Kármán's solution was intuitively satisfying, the solution to the converse problem of a fluid in solid-body rotation above a stationary disk, raised a number of questions concerning its physical reality. Using the same similarity transformation (1), Bödewadt in 1940 (see pp. 213–18 of Schlichting 1968; Fig. 1b) found that the functions (F, G, H) are oscillatory in their approach to the asymptotic values (0,1, 1.4) as $\zeta \rightarrow \infty$. Significantly, $G(\zeta \approx 2.5) \approx 1.26 > 1$ indicating that the tangential velocity near the disk 'overshoots' its value far from the disk. In further contrast with the von Kármán solution, where the boundary layer begins at the origin, the boundary layer in the Bödewadt solution begins at 'infinity' with a presumed infinite supply of mass to the boundary layer; the secondary circulation is completed by mass expelled out of the boundary layer with an axial velocity that is independent of radius. Moreover the form of (1) precludes flow separation as the boundary-layer flow decelerates near the origin, a situation that could not be ruled out on first principles. For these reasons the physical reality of the Bödewadt solution was not to be taken for granted (Moore 1956; Stewartson 1958).

To have a physically realisable version of both the von Kármán and Bödewadt solutions, Stewartson (1958) considered an equivalent pair of problems with a sphere replacing the disk. A rotating sphere in a flow with no rotation at large distance was shown by Stewartson (1958) to behave near the poles like the von Kármán flow with meridional outflow along the sphere's surface from the poles with flow towards the sphere from infinity along the axis of rotation; however in contrast with von Kármán's disc, the equatorward flows from the two poles meet at the equator and continue as radial outflow on the equatorial plane. Conversely in the case of a fluid in solid-body rotation around a stationary sphere, Stewartson (1958) deduced that the flow must be radially inward on the equatorial plane outside the sphere; no solution near the poles was given in this case, although Stewartson (1958) speculates that the Bödewadt solution should be approached there. Using an approximate method valid in the neighborhood of a disk edge, Stewartson (1958) calculated the growth of the boundary layer from the disk edge inward showing that it is qualitatively similar to the solution for flow near the equator on the sphere (cf. his Figs. 3–4); however these solutions did not have any of the characteristics of the Bödewadt solution.

The question of the reality of the Bödewadt solution was finally settled by Rogers and Lance (1964). Following Stewartson (1958), they considered solutions to the boundary-layer equations for a flow in solid-body rotation above a disk of finite radius a; they found, using Stewartson's (1958) power-series expansion, that the solution approaches the Bödewadt solution at $r \approx a/2$ as higher-order terms are added to Stewartson's (1958) zeroth-order solution.

At about the same time (in the 1960s), an educational fluid-mechanics film entitled 'Secondary Flow' by E. S. Taylor experimentally demonstrated the Bödewadt solution (Figs. 4–5 of *Film notes for secondary flow*, web.mit.edu/hml/ncfmf/13SC.pdf).

Solid-body rotation has long occupied a special place in fluid dynamics since it brings considerable simplification to the governing equations. For a Newtonian fluid, the rate of strain $\tau_{r\phi} = \nu r \partial \omega / \partial r = 0$; furthermore the equation for waves on a columnar vortex in solid-body rotation is particularly simple since the stability parameter $r^{-3}\partial(rv)^2/\partial r = 4\omega^2$ (Drazin and Reid, 1981; Chapter 3) is constant. And, as discussed above, there exists the analytical Bödewadt solution for the boundary layer of a fluid in solid-body rotation.

Potential-Vortex Outer Flow

The other canonical case in the consideration of rotating-flow boundary layers is the potential-vortex (the angular momentum per unit mass $rv = \Gamma =$ a constant) outer flow. In this case the stress-divergence term $r^{-2}\partial(r^2\tau_{r\varphi})/\partial r = 0$ while inertial waves are absent since the stability parameter is zero. However, the boundary layer, while not as simple as its solid-body-rotation counterpart, has yielded to analytical/numerical analysis.

The boundary layer of a potential vortex on a finite-radius disk is a special case of the *swirl atomiser* (Fig. 2) first analysed by Taylor (1950). Moore (1956) deduced that similarity solutions of the type discussed above are not possible in this case. Mathematical proof of the nonexistence of such solutions was given by King and Lewellen (1964, p. 1676). In

Fig. 2. A swirl atomiser is represented as the frustum of a cone. Depicted here is an idealised version of this flow with a potential vortex inside the cone. The no-slip condition at the cone wall produces a boundary layer that has, due to the nonzero vertex angle of the cone, lower pressure in the direction of the vertex. Hence an axial flow forms along the cone wall in the boundary layer (indicated in gray shading). The cone devolves to a disk as the vertex angle of the cone approaches $\pi/2$. (After Schlichting 1968.)

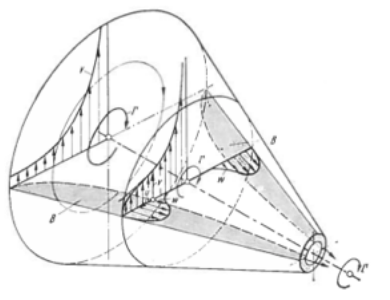

Fig. 3. The boundary-layer profiles of (a) radial, and (b) tangential velocities for a potential vortex for $r/a=0.37(\xi=1)$ and $r/a=0.03(\xi=3.5)$ along with the limiting profiles as $r\rightarrow 0$. (After Burggraf et al. 1971.)

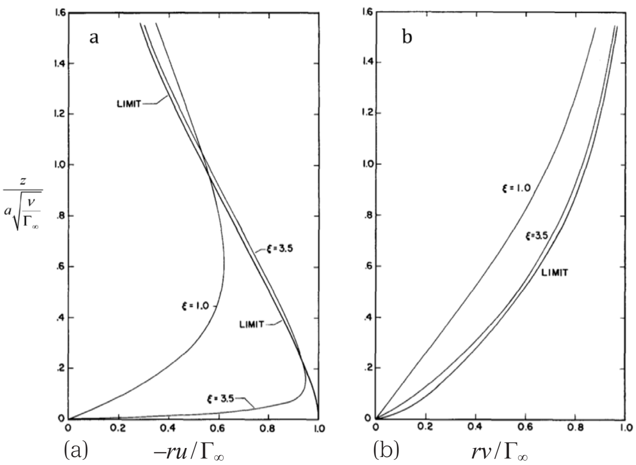

the same proof it was shown that power-law vortices $v \propto r^{\beta}$ do have similarity solutions for $\beta>-1$ and, moreover, must have a tangential-velocity 'overshoot' as does the Bödewadt solution ($\beta=1$).

The first successful numerical calculation of the boundary-layer of a potential vortex on a finite-radius disk was reported by Burggraf, Stewartson and Belcher (1971; BSB). BSB found that the boundary layer has a two-tiered structure (with the tiers delimited by the maximum in $-ru$) as illustrated in Fig. 3, where the coordinate $\xi=-\ln(r/a)$. Figure 3 shows that the maximum in $-ru$ descends with decreasing radius, while rv undergoes a gradual adjustment and reaches 90 per cent of its outer value Γ_∞ over a depth $a\sqrt{\nu/\Gamma_\infty}$. In the limit as $r\rightarrow 0$, the lower tier becomes vanishingly thin leaving just the upper tier, which has the interesting property of having constant head over the depth of the boundary layer and thus is effectively inviscid but yet

Fig. 4. Laser-Doppler velocimeter measurement of the boundary-layer profiles of left) radial and right) tangential velocity for a potential vortex at $r/a=0.1$. Theoretical curve computed for R=5000 compares well to measurements (diamonds). (After Phillips and Khoo 1987.)

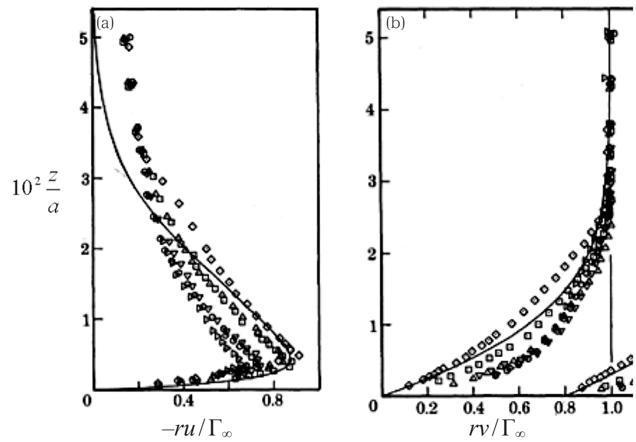

possessing vorticity (see Rotunno 2013 for a more detailed description). Perhaps the most important aspect of the solution seen in Fig. 3 is that the radially inward volume flux increases with decreasing radius, requiring by continuity, fluid to be drawn into the boundary from the outer flow at all radii, in contrast with the Bödewadt solution where the flow is expelled out of the boundary layer at all radii.

Experimental verification of these theoretical results was reported in Phillips and Khoo (1985, Fig. 4). For a Reynolds number $R=\Gamma_\infty/\nu=5000$ the measured flow (diamonds) shows convincing agreement with the theoretical computation in that there is a two-tiered structure and an upper-tier boundary-layer depth $O(R^{-1/2})$. Moreover as a result of the finite inward radial volume flux near the origin, there is a dramatic axial eruption of the boundary layer as shown in the flow visualisation in Fig. 5.

This axial eruption of the boundary layer, the apparent expansion of the vortex, its chaotic merging with the outer flow and visual similarity to tornadoes was first noted in the educational fluid-mechanics film cited above (in this case see Figs. 8–9 of *Film notes for secondary flow*). At about the same time Maxworthy (1971) in an experimental study found similar flows and identified the transition with the vortex breakdown phenomenon (Benjamin 1962). Maxworthy (1971) showed that the kind of gradual adjustment of the outer flow proposed by Lewellen (1962), and further explored in the context of tornadoes by Turner (1966), was only possible for Reynolds numbers much smaller than those occurring in geophysical vortices.

The secondary circulations of the solid-body-rotation (Fig. 1b) and the potential-flow vortex (Fig. 5) are obviously very different. One of the principal objectives of the present study is to understand the factors producing these differing secondary circulations in the more meteorologically relevant case of a Rankine vortex (Bluestein 2013, Chapter 6), which is essentially a combination of the two archetypes discussed above.

Fig. 5. Flow visualisation of the eruption of the potential-flow boundary near the origin (after Phillips 1985). The nondimensional radius $r/a = 0.1$, corresponding to the measurements in Fig. 4., is indicated by the arrow.

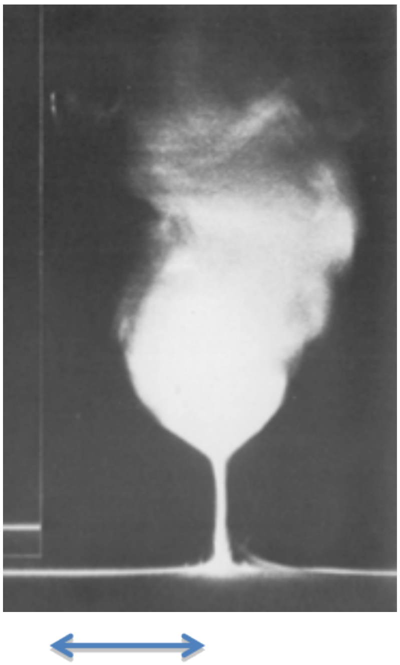

Boundary layer and secondary circulations in a Rankine-like Vortex

Analytical solutions for the boundary layer of a Rankine vortex are unavailable, although certain numerical solutions to truncated systems of equations have been computed (using for example the *momentum integral* technique; see Rott and Lewellen 1966 for a review). In my opinion, the numerical solution of the boundary-layer equations for a Rankine-vortex outer flow, while difficult, is not the most significant challenge; rather it is the effect of the secondary circulation on the outer flow and the possible subsequent feedback to the boundary layer that pose the most daunting conceptual problems. In this section several factors influencing the design of the present numerical experiments are considered.

Now in contrast with the solid-body-rotation or the potential vortex, the Rankine vortex is not a solution to the steady Navier-Stokes equations. So long as there is nonzero viscosity, a Rankine-like vortex will either evolve as for example in

$$\Gamma = \Gamma_\infty \left(1 - \exp(-r^2 / 4\nu t)\right) \qquad \text{...(2)}$$

(t is time) or must be maintained in a steady state by an outer converging flow as for example in the Burgers-Rott vortex,

$$\Gamma = \Gamma_\infty \left(1 - \exp(-br^2 / 2\nu)\right) \quad , \quad u = -br \qquad \text{...(3)}$$

where b is the convergence parameter. For laboratory investigations something like (3) is the universal choice; however there is a variety of methods used to produce the converging flow that would maintain an outer vortex (some of the two-celled variety, see Rotunno 2013) in a steady state, hence each laboratory experiment is somewhat different. Most numerical investigations also choose the latter method to maintain the outer flow, and again, are all somewhat different. A thorough discussion of the general dynamical properties of these vorticies with particular emphasis on the effects of axial variation may be found in Morton (1969).

There was one study, however, that examined the time-dependent problem. Barcilon (1967) studied the time-dependent flow on an infinite domain of an initial vortex in which $\Gamma = \Gamma_\infty$ everywhere except at $z = 0$ and $r = 0$ where $\Gamma = 0$. In the absence of a lower boundary layer, the solution is given by (2); however with the lower no-slip boundary, Barcilon's (1967) formulation captures not only the boundary layer, but also the entire flow interaction between the outer vortex and boundary layer. Barcilon's (1967) analysis, using asymptotic analytical methods, recovered all the important features found in later analyses based on steady-state conditions: axial flow into the boundary layer for $r / \sqrt{\nu t} >> 1$, finite radially inward volume flux in the boundary layer as $r \to 0$, a nearly inviscid, but vortical, flow for $\sqrt{(r^2 + z^2) / \nu t} << 1$ and the necessity for vortex breakdown of the vortex that erupts from the boundary layer.

Inspired by the Barcilon (1967) model, but desiring a solid connection with laboratory studies that take place in a finite-radius container, I will present numerical solutions here to the axisymmetric Navier-Stokes equations, on a domain that includes both the boundary layer and outer flow, for an initial condition given by a Rankine vortex contained within a cylinder of radius a, i.e.,

$$v(r,z) = v_m \begin{cases} r / r_m & 0 \le r \le r_m \\ r_m / r & r_m \le r \le a \end{cases} \quad , \quad u(r,z) = w(r,z) = 0 \qquad \text{...(4)}$$

except at $z = 0$ where instead $v(r,0) = 0$ for all t. By varying r_m, one can examine within the same framework the boundary layer and secondary circulations in outer flows ranging from solid-body rotation to ones approaching potential flow; also all cases have the same angular momentum at $r = a$ ($\Gamma_m = r_m v_m$). Although according to (2) all cases will eventually approach solid-body-rotation outer flow, the following simple estimate shows that the boundary layer reaches its quasi-steady configuration on a much shorter time scale. Estimating from (2) the time needed for viscous effects to bring the entire flow into solid-body rotation as $t_{SB} \sim a^2/\nu$ and the time needed for viscous effects to establish the Burggraf et al. (1971) boundary layer as $t_{BL} \sim a^2/\Gamma_m$, gives $t_{BL} / t_{SB} \sim \nu / \Gamma_m = \mathrm{R}^{-1}$ which is typically small. This prediction of the relatively rapid establishment of the boundary layer and secondary circulation is borne out in the present numerical simulations.

Numerical experiments

Design

To put the problem in non-dimensional form, I define the non-dimensional variables,

$(\hat{r},\hat{z}) = a^{-1}(r,z), \hat{t} = \Gamma_m t / a^2, (\hat{u},\hat{w}) = a\Gamma_m^{-1}(u,w), \hat{\Gamma} = \Gamma_m^{-1}\Gamma, \hat{\varphi} = a^2\Gamma_m^{-2}(p/\rho),$

and, in addition, the non-dimensional vorticity,

$$\left(\hat{\xi},\hat{\eta},\hat{\zeta}\right) = \left(-\frac{1}{\hat{r}}\frac{\partial\hat{\Gamma}}{\partial\hat{z}}, \frac{\partial\hat{u}}{\partial\hat{z}} - \frac{\partial\hat{w}}{\partial\hat{r}}, \frac{1}{\hat{r}}\frac{\partial\hat{\Gamma}}{\partial\hat{r}}\right)$$

The non-dimensional, incompressible, axisymmetric Navier-Stokes equations are therefore:

$$\frac{D\hat{u}}{D\hat{t}} - \frac{\hat{\Gamma}^2}{r^3} = -\frac{\partial\hat{\varphi}}{\partial\hat{r}} + \frac{1}{R}\frac{\partial\hat{\eta}}{\partial\hat{z}} \qquad \text{...(5a)}$$

$$\frac{D\hat{w}}{D\hat{t}} = -\frac{\partial\hat{\varphi}}{\partial\hat{z}} - \frac{1}{R}\frac{1}{\hat{r}}\frac{\partial\hat{r}\hat{\eta}}{\partial\hat{r}} \qquad \text{...(5b)}$$

$$\frac{D\hat{\Gamma}}{D\hat{t}} = +\frac{\hat{r}}{R}\left(\frac{\partial\hat{\zeta}}{\partial\hat{r}} - \frac{\partial\hat{\xi}}{\partial\hat{z}}\right) \qquad \text{...(5c)}$$

$$\frac{1}{\hat{r}}\frac{\partial\hat{r}\hat{u}}{\partial\hat{r}} + \frac{\partial\hat{w}}{\partial\hat{z}} = 0 \qquad \text{...(5d)}$$

where $D/D\hat{t} = \partial/\partial\hat{t} + \hat{u}\partial/\partial\hat{r} + \hat{w}\partial/\partial\hat{z}$. The initial condition (4) becomes

$$\hat{\Gamma}(\hat{r},\hat{z}) = \begin{cases} \hat{r}^2/\hat{r}_m^2 & 0 \le \hat{r} \le \hat{r}_m \\ 1 & \hat{r}_m \le \hat{r} \le 1 \end{cases}, \quad \hat{u}(\hat{r},\hat{z}) = \hat{w}(\hat{r},\hat{z}) = 0 \qquad \text{...(6)}$$

where $\hat{r}_m = r_m/a$. It is clear from (5)–(6) that the solutions will depend on the two nondimensional numbers, $(R,\hat{r}_m)$.

The design of the present experiments is intended to simulate the response of a fluid with initial motion described by (6), to a sudden imposition of the no-slip condition at the lower boundary $\hat{z} = 0$. The container continues to rotate and impart angular velocity to the fluid at $\hat{r}=1$; however the fluid is allowed to slip freely in the axial direction, as is the case in the idealised analytical problems discussed by Stewartson (1958); the same type of stress conditions are applied at $\hat{r}=0$. To provide a closer correspondence with these idealised analytical problems, the ideal situation in the present numerical experiments would be to have an infinitely long domain in the axial direction. Since this is not possible one often resorts to 'open' boundary conditions, which unfortunately introduce uncertainty (Fiedler 1995).

To avoid this uncertainty and to prevent the formation of boundary layers at the upper boundary, I have specified boundary conditions that yield a closed container, with free-slip conditions along the top edge, which in the present study we have set at $\hat{z} = 4$. The domain and boundary conditions are shown in Fig. 6.

The boundary conditions just described allow a few general remarks on what can be expected of the secondary circulation. If one computes the secondary circulation (going clockwise) around the domain edge, $\hat{C} = \oint \hat{\boldsymbol{u}} \bullet d\hat{\boldsymbol{s}}$ from the first two equations of (5) and applies the boundary conditions, the result is,

$$\frac{\partial\hat{C}}{\partial\hat{t}} = \int_0^1 \hat{r}^{-3}\hat{\Gamma}^2(\hat{r},\hat{z}_t)d\hat{r} + \oint \hat{\boldsymbol{F}} \bullet d\hat{\boldsymbol{s}} \qquad \text{...(7)}$$

Fig. 6. Domain and boundary conditions for the present numerical experiments.

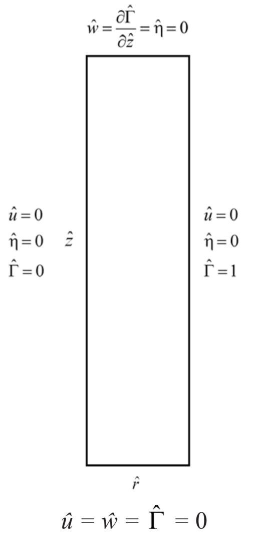

where $\hat{\boldsymbol{F}}$ represents the frictional terms on the boundaries. Equation (7) indicates that a steady motion $\partial\hat{C}/\partial\hat{t} = 0$ is possible if the integrated centrifugal force (first term on the rhs) at the top boundary is maintained and balanced by the integrated boundary drag. (In the present case most of the contribution to the boundary-drag term comes from the lower boundary.) In the case of solid-body rotation ($\hat{r}_m = 1$), the simulations show that the initial radial distribution of $\hat{\Gamma}$ is maintained in a quasi steady state by frictional diffusion balancing advection of $\hat{\Gamma}$ in the upper part of the domain.

The numerical model used here is described by Rotunno (1979); in that model (5a) and (5b) are combined to give

$$\hat{r}\frac{D}{D\hat{t}}\frac{\hat{\eta}}{\hat{r}} = \frac{1}{\hat{r}^3}\frac{\partial\hat{\Gamma}^2}{\partial\hat{z}} + \frac{1}{R}\left(\frac{\partial^2\hat{\eta}}{\partial\hat{z}^2} + \frac{\partial}{\partial\hat{r}}\frac{1}{\hat{r}}\frac{\partial\hat{r}\hat{\eta}}{\partial\hat{r}}\right) \qquad \text{...(8)}$$

and (5d) is replaced by

$$(\hat{u},\hat{w}) = \left(\frac{1}{\hat{r}}\frac{\partial\hat{\psi}}{\partial\hat{z}}, -\frac{1}{\hat{r}}\frac{\partial\hat{\psi}}{\partial\hat{r}}\right) \qquad \text{...(9)}$$

and the definition

$$\hat{r}\hat{\eta} = \frac{\partial^2\hat{\psi}}{\partial\hat{z}^2} + \hat{r}\frac{\partial}{\partial\hat{r}}\frac{1}{\hat{r}}\frac{\partial\hat{\psi}}{\partial\hat{r}} \quad . \qquad \text{...(10)}$$

This 'streamfunction-vorticity' system has two prognostic equations (8) and (5c) and one diagnostic equation (10) for the three unknowns. The finite-difference versions of these equations are computed on a grid of equally spaced points with $\Delta\hat{r} = \Delta\hat{z} = 1/120$; all simulations reported on here are carried out with $R=1000$ and therefore are well resolved (since $\Delta\hat{r} << R^{-1/2}$).

One further modeling device was necessary. The initial adjustment of the interior flow to the no-slip boundary condition introduces vertically propagating inertial waves; left unmodified they would reflect off the upper boundary and eventually return to distort the boundary-layer-outer-flow interaction that is the subject of our study. To eliminate these waves, I have implemented a Rayleigh damping term $-\alpha(\hat{z})\hat{\eta}$ to the rhs of (8) and $-\alpha(\hat{z})\left(\Gamma-\Gamma_0(\hat{r},\hat{t})\right)$ to the rhs of (5c) where $\alpha(\hat{z})=(\hat{z}=2)$ for $\hat{z}\geq 2$ (otherwise it is zero) and $\hat{\Gamma}_0(\hat{r},\hat{t})$ is the evolving distribution due to radial viscous diffusion [i.e $\partial_{\hat{t}}\hat{\Gamma}_0=R^{-1}\hat{r}\partial_{\hat{r}}(\hat{r}^{-1}\partial_{\hat{r}}\hat{\Gamma}_0)$] and is solved for numerically during the course of the integration. In this way inertial waves can be damped relative to the diffusively evolving part of $\hat{\Gamma}(\hat{r},\hat{t})$.

Results

The results for solid-body rotation ($\hat{r}_m$=1) are considered first. Figure 7 shows the steady-state velocity components on the subdomain, $0\leq\hat{r}\leq 1, 0\leq\hat{z}\leq 1$.

For $\hat{r}$ less than approximately ½, it is clear that the velocity fields have the qualitative character of the Bödewadt solution; Fig. 8 makes a direct comparison of the current numerical solution with the Bödewadt solution in the vertical coordinate $\varsigma=z\sqrt{\omega/\nu}=(z/a)\sqrt{\Gamma_m/\nu}=\hat{z}R^{1/2}$. Clearly the Bödewadt solution is also quantitatively valid for the center part of the disc as found by Rogers and Lance (1964).

The presence of a finite disk edge thus does not cause any major disruption of the picture provided by the Bödewadt solution: mass and angular momentum are supplied from above and beyond a radius of approximately ¾ (also predicted in Rogers and Lance 1964) instead of from infinite radius. Inward of the ¾ radius, mass and angular momentum are expelled in a manner that is consistent with the solid-body-rotation outer flow.

The situation is radically different for the Rankine vortex. Since, as discussed above, the solution is fundamentally time-dependent, Fig. 9 shows the velocity fields at $\hat{t}$=1,10 and 100. As predicted at the end of the preceding section, the time scale for the boundary layer is $t_{BL}\sim a^2/\Gamma_m$, which, in nondimensional terms, occurs at $\hat{t}$=1; Fig. 9 indicates that the boundary-layer depth changes very little past this time. Also, as time advances the solid-body-rotation part of the inner core expands so that the flow at $\hat{t}$=100 begins to resemble that in Fig. 7. Further integration out to nondimensional times of several hundred shows the flow asymptotically reaches that shown in Fig. 7 (which is consistent with our estimate $t_{SB}\simeq a^2/\nu\rightarrow\hat{t}_{SB}\simeq R=1000$ in the present case).

Fig. 7. Steady state velocity fields for the case of solid-body rotation. Contour levels are 0.025 for $\hat{u}$, 0.1 for $\hat{v}$ and 0.02 for $\hat{w}$; here and throughout red signifies negative and blue positive values of the fields (black is the zero line).

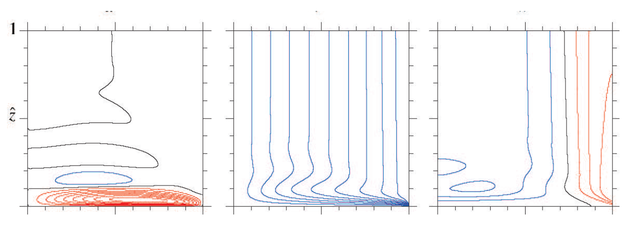

Broadly speaking the boundary layer of the Rankine vortex appears to be a conjoining of the Bödewadt boundary layer (Fig. 1b), with vertical oscillations extending above, and the potential-vortex boundary layer (Fig. 5), without such oscillations. However, closer examination reveals that the oscillations in the vortex core have larger amplitudes and are more irregular than their Bödewadt counterparts. This irregularity and the general character of the velocity field, which evinces a very strong low-level inflow, vertical motion and then outflow near the 'corner' region (near $\hat{r}=\hat{z}=0$), is the hallmark of the 'vortex breakdown' phenomenon mentioned above. The flow morphology is illustrated in Fig. 10 which shows $\hat{\psi}$ (cf. Fig. 5) and $\hat{\Gamma}$ at $\hat{t}$=1. The streamline pattern indicates a secondary flow into the boundary layer from above in the region where the angular momentum of the outer flow is relatively constant; the vortex core exhibits the folding of the angular momentum surfaces that is a prelude to instability and thus a contributor to the irregular motions in evidence. All of these features are consistent with Barcilon's (1967) analysis on an infinite domain.

It is of interest to view the solutions shown in Fig. 10 in the more traditional form of velocity profiles along the radius of the disk. Figure 11 shows the velocity profiles plotted as in Fig. 8 for the five stations $\hat{r}$ = 0.1, 0.3, 0.5, 0.7, 0.9 at $\hat{r}$=10. Beginning from the outermost position, Figs. 11c–e indicate an oscillation-free, intensifying-flow boundary layer with decreasing radius, consistent with the BSB terminal boundary layer for a potential vortex (Fig. 3). Approaching the inner-core region in Fig. 11b, one sees vertical oscillations that are qualitatively similar to those of the Bödewadt solution but are less attenuated with distance above the disk; at the innermost position (Fig. 11a), the oscillations are more attenuated and evince a smaller wavelength, consistent with the fact that for the Rankine vortex, the local rotation

Fig. 8. Comparison of velocity profiles (thin lines for $\hat{r}$=0.1, 0.3, 0.5, 0.7) from the solid-body-rotation simulation with those of the Bödewadt solution (dark line). Agreement of the model with Bödewadt increases for decreasing radius.

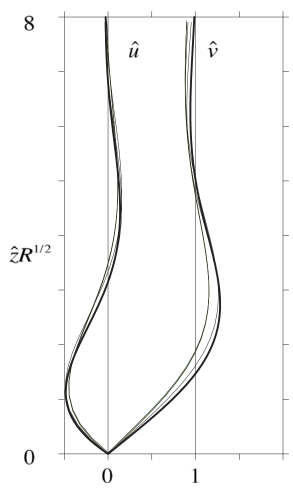

Fig. 9. Velocity field for an initial vortex given by (6) with $\hat{r}_m = 0.25$ for $\hat{t} = 1$ (first row, contour levels are 0.5 for $\hat{u}$, 0.5 for $\hat{v}$ and 0.5/0.05 for positive/negative $\hat{w}$), $\hat{t} = 10$ (second row, same contour levels as for $\hat{t} = 10$) and $\hat{t} = 100$ (last row, contour levels are 0.1 for $\hat{u}$, 0.1 for $\hat{v}$ and 0.02 for $\hat{w}$).

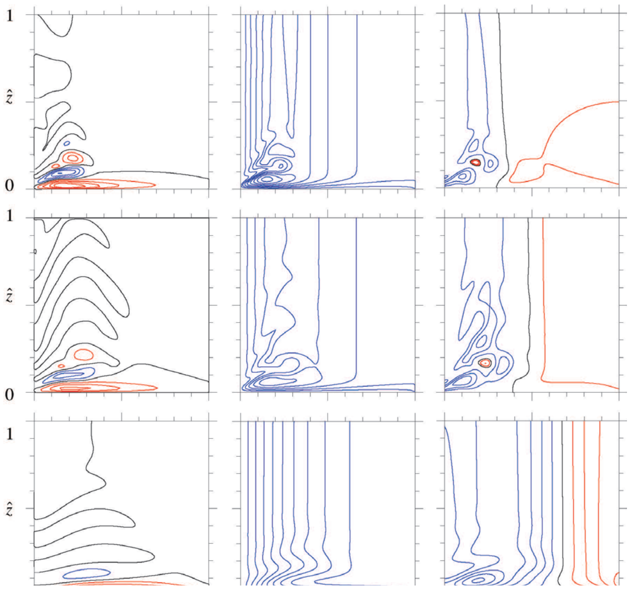

Fig. 10 Streamfunction and angular momentum for $\hat{t} = 1$. Contour intervals are 0.003 for the streamfunction and 0.1 for the angular momentum.

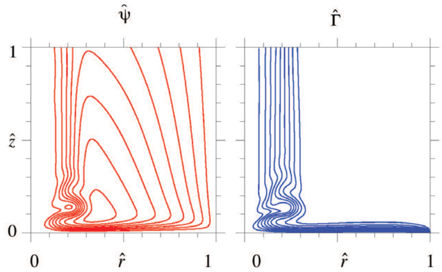

rate ($\omega = \Gamma_m / r_m^2$) is greater than it is in the Bödewadt case ($\omega = \Gamma_m / a^2$) and hence the length scale of the oscillations, $\sqrt{\nu / \omega}$, is smaller. Note, however, that the tangential velocity in the boundary layer 'overshoots' the outer flow directly above it by a far greater degree (by approximately a factor of two seen in Fig. 11a) than it does in the Bödewadt solution (by approximately 26%, see Fig. 8); however the overshoot calculated by the ratio of the boundary-layer tangential-wind maximum to the outer-flow maximum (at larger radius) stays roughly at 25% (Fig. 9).

The present experiments indicate that the amplitude of the oscillations and instability seen in Fig. 10 increase as $\hat{r}_m \to 0$ whereas they decrease and the solution approaches the Bödewadt solution (Fig. 7) as $\hat{r}_m \to 1$. The following simple explanation seems to fit the available facts. Consider first the case of solid-body rotation. For a closed cylinder there are inertial waves that propagate information in the axial direction. Following the development in Batchelor (1967, p. 566), the criterion for upstream axial wave propagation is

$$\frac{W}{a\omega} < 0.52 \qquad \text{...(11)}$$

in the present notation and with W denoting the constant axial flow speed. The Bödewadt solution has $W \simeq 1.4\sqrt{\nu\omega}$ which when combined with (11) gives the criterion, $R > 7.3$, which is easily satisfied in the present simulations. Hence the outer flow can adjust to information supplied to it by the boundary layer and vice-versa in regions of upward flow, while in regions of downward flow the boundary layer adjusts to the information coming from the outer flow. Thus in the context established by Benjamin (1962) the Bödewadt solution is subcritical and information can freely propagate upstream and downstream along the axial direction.

For the Rankine vortex, however, the situation is fundamentally different. For the region $\hat{r}_m \le \hat{r} \le 1$ the boundary layer approximates that of the potential vortex found by BSB which as noted above has a finite positive value of $-\hat{r}\hat{u}$ as $\hat{r} \to 0$; however since $\hat{r}\hat{u}$ must be zero at the origin, there must exist large convergence in the corner region and an intense

Fig. 11. Velocity profiles $(\hat{u}, \hat{v})$ at $\hat{t} = 10$ for $\hat{r} = (a)0.1, (b)0.3, (c)0.5, (d)0.7, (e)0.9$. The radial component curve is green. The velocity scale ranges from -4 to +4 units.

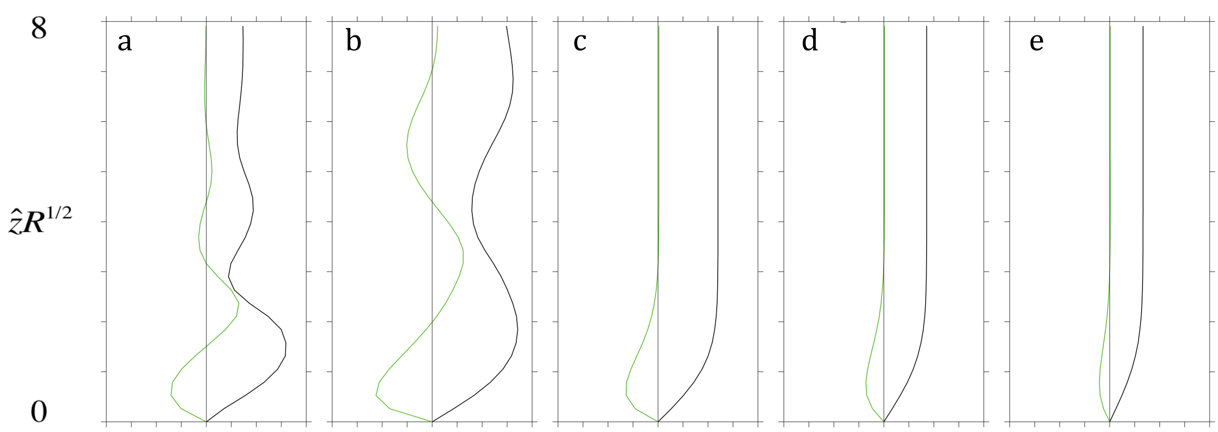

upward vertical jet emerging from the boundary layer, as seen in Fig. 9. Further analysis of similar flows indicates that this vertical jet is supercritical (Rotunno 1979; Fiedler and Rotunno 1985) and that a smooth transition of the boundary-layer-produced vortex to the outer flow is not possible in the Rankine-vortex core.

One final feature of the secondary circulation of the Rankine vortex can be deduced as follows: According to boundary-layer theory the radial pressure gradient is nearly independent of vertical distance above the lower boundary; hence (5a) evaluated at $\hat{z}=0$ is

$$\frac{\partial\hat{\varphi}}{\partial\hat{r}} = \frac{1}{R}\frac{\partial\hat{\eta}}{\partial\hat{z}}\bigg|_{\hat{z}=0} \quad , \qquad \text{...(12)}$$

the physical meaning of which was the subject of an enlightening essay by Morton (1984). To estimate the basic dependencies of the non-dimensional boundary-layer volume-flow rate, one can substitute $\hat{r}^{-1}v_0^2$ for the radial pressure gradient and approximate $\hat{\eta}$ by $\partial_{\hat{z}}u$ in (12) to deduce $\hat{r}\hat{u} \sim -v_0^2(\hat{r},\hat{t})\hat{\delta}^2$ (hence the radial flow is always inward) and with (5d) that

$$\hat{w}(\hat{r},\infty,\hat{t}) \sim \hat{r}^{-1}\,\partial[\hat{v}_0^2(\hat{r},\hat{t})\hat{\delta}^2]/\partial\hat{r} \qquad \text{...(13)}$$

For a boundary-layer thickness $\hat{\delta}$ that is roughly constant with radius, (13) indicates that the axial motion changes sign at the radius where the outer-flow tangential wind has its maximum value; this prediction is roughly consistent with the results shown in Fig. 9 at the earlier times. For the case of solid-body rotation the maximum value of $\hat{v}_0$ is at the outer radius and so in this case, according to (13), the inward increase of $\hat{\delta}$ must determine the point at which the axial motion changes sign.

Comments on atmospheric vortices

In the context of geophysical fluid dynamics, the present discussion is mainly applicable to cases where the outer (primary) circulation is produced by a process that is external to the boundary layer. For the supercell tornado, the parent rotating thunderstorm is the source of the outer circulation (Rotunno 2013); for nonsupercell tornadoes and waterspouts, a pre-existing line of horizontal shear is thought to be the outer-rotation source (Simpson et al. 1986; Wakimoto and Wilson 1989). For a midlatitude cyclone, baroclinic waves produce perturbations to the local rotation rate of the atmosphere that produce the Ekman layer (which is a linearised version of the Bödewadt boundary layer).

The hurricane, although sharing some of the features of the above-mentioned geophysical vortices, is distinctly different in several respects. Perhaps the most important difference is that the hurricane-boundary-layer secondary circulation influences not just the outer primary circulation, but also the outer-flow buoyancy (entropy) distribution which is essential. Emanuel (1986) presents a theory for the axisymmetric steady-state hurricane in which the primary circulation is in gradient-wind balance; a simple boundary-layer model is used to provide the necessary closure on the relation between entropy and angular momentum. As mentioned in the Introduction, hurricane boundary layers are expected and observed to have supergradient winds, however the effect of the latter on relations between entropy and angular momentum derived from simple boundary-layer models such as in the Emanuel theory, was estimated to be small in the steady-state solutions found in an axisymmetric high-resolution numerical modeling study (Bryan and Rotunno 2009). On the other hand, the gradient-wind assumption does eliminate the oscillations in angular momentum seen here (Fig. 10) and in recent high-resolution hurricane simulations (Fig. 4b of Bryan and Rotunno 2009); the latter oscillations are associated with the tangential-wind 'overshoot' in the boundary layer and therefore their elimination leads to an underestimation of the maximum possible tangential wind. Finally in order to have a clearer picture of the relation between the hurricane outer, primary circulation and the boundary-layer-induced secondary circulation, the concepts of sub/supercritical flow (used herein) can be applied only if a theory of (vertical-radial) wave propagation on the hurricane vortex can be developed. I think these considerations will be especially important in discussions of hurricane intensification (Montgomery and Smith 2014).

Concluding remarks

Although easy to understand at qualitative level, quantitative results on secondary circulations in physically realisable rotating-flow boundary layers have been hard to come by. While the Bödewadt similarity solution (1) is the bedrock of quantitative knowledge in this area, the requirement of an infinite domain with infinite horizontal velocity at infinite radius renders impossible exact experimental verification. The boundary layer of a potential vortex on a disk of finite radius is also well understood (Fig. 4; Burgraff et al. 1971) however it too would be impossible to verify exactly in an experiment due to the impossibility of having infinite velocity at the origin. The present study aims to take a small step towards experimentally possible versions of these flows by carrying out numerical solutions of the axisymmetric Navier-Stokes equations in a finite cylindrical domain and by allowing for a time-dependent flow.

The present strategy is therefore to study the evolution of the Rankine vortex (4), which has a solid-body-rotation core and a potential-vortex exterior, subject to the sudden initial imposition of the no-slip condition at the lower boundary. With the radius of maximum wind located at the boundary ($r_m=a$), (4) describes a fluid in solid-body rotation in the entire cylinder; the present results indicate a steady solution that is quantitatively similar to the Bödewadt solution over approximately the inner ¾ of the domain. The numerical solutions show that the secondary circulation takes the form of flow into the boundary layer beyond a radius of approximately ¾ of the disk radius and then assumes the upward flow of the Bödewadt solution inward of that point, consistent with the results obtained through the asymptotic expansions of Rogers and Lance (1964). As in the Bödewadt solution, the present finite-radius simulations show that the primary outer-flow vortex is completely compatible with the secondary flow.

With the radius of maximum wind located within the disc radius ($r_m<a$), (4) describes a Rankine vortex. In this case the outer vortex evolves (primarily through horizontal diffusion), however the boundary layer takes its form relatively quickly. That boundary layer is consistent with the potential-vortex boundary layer described in Burggraf et al. (1971) for $r_m < r < a$. However for $0 < r < r_m$ there is only a qualitative similarity to the Bödewadt solution; here the solution exhibits intense inflow and then upward flow in the corner region with a sudden transition to the outer flow through a vortex breakdown. These findings are completely in accord with the seminal paper study by Barcilon (1967) of the evolution of the vortex (4) (in the limit $r_m \to 0$) on an infinite domain.

Acknowledgments

Thanks are due to Roger Smith and Mike Montgomery for their thorough formal reviews of this paper and to George Bryan, Brian Fiedler and David Nolan for their comments on its first draft.

Bruce Morton was well known for his passion for the subject of vorticity and, in particular, the use of the latter concept in the study of vorticies and boundary layers. This article is written in fond remembrance of the many illuminating and trenchant insights Bruce Morton shared with me.

References

Barcilon, A. I. 1967. Vortex decay above a stationary boundary. *J. Fluid Mech., 27*, 155–75.

Batchelor. G. K. 1967. *An introduction to fluid dynamics*, Cambridge, 615pp.

Benjamin, T. B. 1962. Theory of vortex breakdown. *J. Fluid Mech., 14*, 593–629.

Bluestein, H. B. 2013. *Severe convective storms and tornadoes*, Springer, 456pp.

Burggraf, O. R., Stewartson, K. and Belcher, R. 1971. *Phys. Fluids, 14*, 1821–33.

Bryan, G. H. and Rotunno, R. 2009. Evaluation of an analytical model for the maximum intensity of tropical cyclones. *J. Atmos. Sci., 66*, 3042–2060.

Drazin, P. G. and Reid, W. H. 1981. *Hydrodynamic instability*. Cambridge, 527pp.

Duck, P. W. and Foster, M. R. 2001. Spin-up of homogeneous and stratified fluids. *Annu. Rev. Fluid Mech.,33*, 231–63.

Emanuel, K. A. 1986. An air-sea interaction theory for tropical cyclones. Part I: Steady-state maintenance. *J. Atmos. Sci., 43*, 585–604.

Fiedler, B. H. 1995. On modeling tornadoes in isolation from the parent storm. *Atmos. Ocean, 32*, 335–59.

Fiedler, B. H. and Rotunno, R. 1986. A theory for maximum windspeeds in tornado-like vorticies. *J. Atmos Sci., 43*, 2328–40.

King, W. S. and Lewellen, W.S. 1964. Boundary-layer similarity solutions for rotating flows with and without magnetic interaction. *Phys. Fluids, 7*, 1674–80.

Lewellen, W. S. 1962. A solution for three-dimensional vortex flows with strong circulation. *J. Fluid Mech., 14* , 420–32.

Maxworthy, T. 1971. On the structure of concentrated, columnar vortices. *Astronautica Acta, 17*, 363–74.

Montgomery, M. T. and Smith, R. K. 2013. Paradigms for tropical-cyclone intensification. *Aust. Met. Oceanogr. J., (64)*. 40–70.

Moore, F. K. 1956. Three-dimensional boundary layer theory, *Advances in applied mechanics*, 4, Academic Press, 160–224.

Morton, B. R. 1969. The strength of vortex and swirling core flows. *J. Fluid Mech., 38*, 315–33.

Morton, B. R. 1984. The generation and decay of vorticity. *Geophys. Astrophys. Fluid Dynamics, 28*, 277–308.

Pedlosky, J. 1984. *Geophysical fluid dynamics*. Springer-Verlag. 624pp.

Phillips, W. R. C. 1985. On vortex boundary layers. *Proc. R. Soc. Lond., A400*, 253–61.

Phillips, W. R. C. and Khoo, B. C. 1987. The boundary layer beneath a Rankine-like vortex. *Proc. R. Soc. Lond., A411*, 177–92.

Rogers, M. H. and Lance, G. N. 1964. The boundary layer on a disc of finite radius in a rotating fluid. *Quart. J. Mech. Appl. Math., 17*, 319–30.

Rott, N. and Lewellen, W.S. 1966. Boundary layers and their interactions in rotating flow. *Prog. Aero. Sci., 7*, 111–144.

Rotunno, R. 1979. A study in tornado-like vortex dynamics. *J. Atmos Sci., 36*, 140–55.

Rotunno, R. 2013. The fluid dynamics of tornadoes. *Ann. Rev. Fluid Mech., 45*, 59–84.

Schlichting, H. 1968. *Boundary-layer theory*, McGraw-Hill, 748pp.

Simpson, J., Morton, B. R., McCumber, M. C., Penc, R. S. 1986. Observations and mechanisms of GATE waterspouts. *J. Atmos. Sci.. 23*, 1465–68.

Smith, R.K. and M. Montgomery, M. T. 2008. Balanced boundary layers in hurricane models. *Quart. J. Roy. Met Soc., 134*, 1385–95.

Stewartson, K. 1958. On rotating laminar boundary layers. *Boundary layer research*, Springer-Verlag, 59–71.

Taylor, G. I. 1950. The boundary layer in the converging nozzle of a swirl atomizer. *Quart. J. Mech. Appl. Math., 3*, 129–39.

Turner, J. S. 1966. The constraints imposed on tornado-like vortices by the top and bottom boundary conditions. *J. Fluid Mech., 25*, 377–400.

Wakimoto, R. M. and Wilson, J. W. 1989. Non-supercell tornadoes. *Mon. Wea. Rev., 117*, 1113–40.